Theor Chem Account (2007) 118:623–630
DOI 10.1007/s00214-007-0348-9

REGULAR ARTICLE

$4p^2$ resonances in photoionization from $4s4p$ levels in neutral zinc

Charlotte Froese Fischer · Oleg Zatsarinny

Received: 7 February 2007 / Accepted: 13 March 2007 / Published online: 23 June 2007

Abstract In neutral zinc the $4p^2$ configuration lies above the $3d^{10}4s$ ionization limit and its levels become perturbers in the continuum. Lines have been identified in the Zn I spectrum for the $4s4p\ ^3P^\circ - 4p^2\ ^3P$ multiplet, whereas no lines have been found for transitions to $4p^2\ ^1D$ or ^1S. In this paper, cross sections for photoionization from $4s4p$ levels are reported that reveal the positions and widths of the $4p^2$ resonances. Calculations were performed using the multiconfiguration Hartree-Fock (MCHF) and B-spline R-matrix (BSR) method. Results from Breit–Pauli calculations that ignore the background continua are also presented. Included in the latter are energies for the $4s^2\ ^1S_0$, $4s4p\ ^1P^\circ_1$, $^3P^\circ_{1,2,3}$, $4s4d\ ^1D_2$, $4p^2\ ^3P_{1,2,3}$, $^1D_2$ and $^1S_0$ levels and transition data (transition energies, line strengths, f-values, and A-rates) for all E1 transitions between these levels. Transition energies and the agreement in the length and velocity values, particularly for allowed transitions, indicate the accuracy of the computational model. Line widths are compared with other estimates.

Keywords Atoms · Correlation · Energy levels · Photoionization cross sections · Transition probabilities

Contribution to the Serafin Fraga Memorial Issue.

C. Froese Fischer (✉)
National Institute of Standards and Technology,
Gaithersburg, MD 20899-8422, USA
e-mail: charlotte.f.fischer@vanderbilt.edu;
Charlotte.Fischer@Nist.Gov

O. Zatsarinny
Department of Physics and Astronomy, Drake University,
Des Moines, IA 50311, USA

1 Introduction

The ground state of neutral zinc is $3d^{10}4s^2$ and the $4p^2$ configuration lies above the $3d^{10}4s$ ionization limit. In 1925 Sawyer and Reese [1] identified lines in the observed Zn I spectrum as belonging to the $4s4p\ ^3P^o - 4p^2\ ^3P$ multiplet in spite of the upper levels being above the ionization limit. They noted that two of the lines had a diffuse character (see Fig. 1 of Ref. [2]). In 1929 Selwyn [3] tentatively identified these as transitions to $4p^2\ ^3P_2$ and shortly thereafter, in 1931, Majorana [4] provided the first explanation of the line width, introducing the notion of radiationless decay into the continuum. A definitive theoretical description of this process, now referred to as autoionization [5], was presented in 1961 by Fano [6]. Often this process is described in terms of non-relativistic theory, invoking at most the spin–orbit operator which is one of the relativistic operators of the Breit–Pauli Hamiltonian [7]. In 1970 Martin and Kaufman [2] derived the positions of the $4p^2\ ^3P$ levels and also measured the width of the $^3P_2$ level as being $21.7\,\mathrm{cm}^{-1}$. From a simple intermediate coupling calculation they estimated the width of the $4p^2\ ^1D_2$ and $^1S_0$ levels to be $6{,}800\,\mathrm{cm}^{-1}$ and $<170\,\mathrm{cm}^{-1}$, respectively. The $^1D_2$ and $^1S_0$ levels have not as yet been identified.

Early theoretical studies of Zn were non-relativistic. In multiconfiguration Hartree-Fock (MCHF) calculations for $4s^2\ ^1S$ – $4s4p\ ^1P$ transitions in the Zn iso-electronic sequence, Froese Fischer and Hansen [8] found that core-valence correlation decreased the oscillator strength by 11 % in the neutral atom. Subsequent studies for ^1D states [9] found strong configuration interaction between $4s4d$ and $4p^2$ configuration states. Only results for the $4s4d\ ^1D$ level were reported for Zn. Completely missing was information about the $4p^2\ ^1D$ level. More recent studies have included relativistic effects, although a number of publications for the

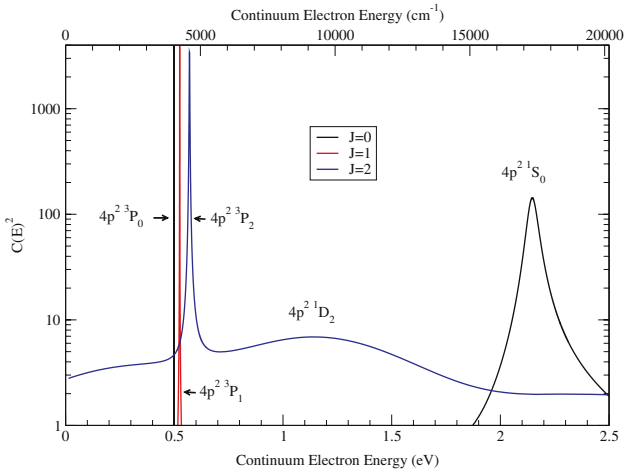

Fig. 1 $C(E)^2$ for the even parity $J = 0, 1, 2$ wave functions as a function of the energy of the continuum electron

sequence report limited information for the neutral atom [10, 11]. Of particular interest are the autoionizing widths found by Chantepie et al. [12] from fully relativistic calculations for $4p^2\ ^3P_{0,1,2}$ to be 0.020, 0.31, and 23 cm^{-1}, respectively, for these three levels.

This paper begins with an investigation of the properties of the wave functions for the $4p^2\ ^3P_{0,1,2}$, $^1D_2$, and $^1S_0$ states when interaction with the continuum is neglected. Both correlation and relativistic effects are found to be important. To complete the study, energy levels are also determined for $4s^2$, $4s4d\ ^1D_2$, and all levels of $4s4p$. Transition probabilities for all possible E1 transitions between levels are reported. Comparison of computed and observed transition energies and agreement in length and velocity forms of the oscillator strengths for allowed transitions, provide a measure of the accuracy of the theoretical wave functions. The calculations are then extended by using the B-spline R-matrix (BSR) method [13] to first compute the even parity continuum wave functions for $J = 0, 1, 2$ in the energy region of the $4p^2$ perturbers and then the cross sections for photoionization from the $4s4p$ levels. The weights of the perturbers reveal the positions and widths of the resonances. These will be compared with observation and other theory. Photoionization cross sections that show the position of resonances as a function of wavelength will also be presented.

2 Background theory

According to Fano's theory [6], described more recently in standard texts [14,15], the wave function for a state in the continuum with a total energy E can be partitioned into a continuum component and a bound component of finite radius, namely

$$\Psi(\gamma\ LS; E) = \Psi_c(\gamma_c\ LS; E) + \Psi_b^u(\gamma_b\ LS). \tag{1}$$

In this definition, $\Psi_c(\gamma_c\ LS; E)$ is the energy dependent continuum portion with the label $(\gamma_c\ LS)$ while $\Psi_b^u(\gamma_b\ LS)$ is an unnormalized bound portion with the label $(\gamma_b\ LS)$. The $4p^2$ levels are all below the $3d^{10}4p$ ionization limit so that the continuum portions are restricted to $4skl\ LS$ channel functions, with the radial function $P_{kl}(r)$ for the one-electron continuum function normalized so that

$$P_{kl}(r) \to \sqrt{\frac{2}{k\pi}}\,[F_{kl}(r)\cos\delta_l + G_{kl}(r)\sin\delta_l]\,, \tag{2}$$

asymptotically at large r. In this definition the functions $F_{kl}(r)$ and $G_{kl}(r)$ are regular and irregular Coulomb functions, δ_l is the short-range phase shift, and $k^2 = 2(E - E_0)$ is the energy of the one-electron continuum function, in Rydbergs, with the total energy E and the $3d^{10}4s$ ionization limit E_0 in atomic units. It is convenient to express the contribution to the wave function from the bound component in terms of a normalized function by introducing an energy dependent coefficient $C(E)$ so that

$$\Psi_b^u(\gamma_b\ LS; E) = C(E)\Psi_b^n(\gamma_b\ LS; E), \tag{3}$$

where the superscripts u and n refer to unnormalized and normalized functions, respectively. Then $C(E)^2$ is the weight of the perturber in the continuum wave function. In the spline-Galerkin method applied by Brage et al. [16] to the calculation of positions and widths for bound states in the continuum of He and H^- such as $2s2p$, the function $C(E)^2$ determined the position and the width of the resonance. This method allows the perturber to be a function of the energy and is the method used in the present paper.

Often the bound component is assumed to be independent of E and then, by the "Golden Rule" [14,15], the width at half height of the resonance is

$$\Gamma = 2\pi\,\langle\Psi_c(\gamma_c\ LS; E)\mid H - E \mid \Psi_b^n(\gamma_b\ LS)\rangle^2 \tag{4}$$

and the autoionization rate (in seconds) is

$$A = \frac{2\pi}{\hbar}\langle\Psi_c(\gamma_c\ LS; E)\mid H - E \mid \Psi_b^n(\gamma_b\ LS)\rangle^2. \tag{5}$$

When the bound and continuum components are orthogonal, Γ is proportional to the square of the interaction matrix element where, for our purposes, the Hamiltonian H is the Breit–Pauli Hamiltonian.

At this point it is important to remember that the many-electron Hamiltonian for Zn, has both a discrete spectrum and continuous spectrum. Of interest is that portion of the continuous spectrum for which the wave function has a significant $4p^2$ component. The discussion so far has been independent of any physical process. With reference to photoionization, the presence of a $4p^2$ component distributes the cross section

for excitation from a given initial state to an energy range. The energy, k^2, of the one-electron continuum function is the energy of the ejected electron, usually given in eV in experiment. The same wave function may be used to describe other physical processes such as radiative decay. For this reason we shall refer to k^2 as the continuum electron energy which, by definition, is the total energy relative to the $3d^{10}4s$ ionization limit.

In this paper we investigate the nature of the bound component to explain why the $4s4p\ ^3P^o - 4p^2\ ^3P$ multiplet is observed with a noticeable line width for transitions to $^3P_2$, whereas no line has been identified for the $4s4p\ ^1P_1^o - 4p^2\ ^1D_2$ or the $4s4p\ ^1P_1^o - 4p^2\ ^1S_0$ transition. As predicted by Majorana, the line width for transitions to the $^3P_2$ level is due to a relativistic effect arising primarily from the spin–orbit operator, thereby giving the bound portion of the $^3P_2$ level a $^1D_2$ component. It will be shown that $^3P_1$ also acquires some width.

3 Computational method

A Breit–Pauli calculation includes relativistic effects to first-order in α^2, where α is the fine-structure constant. It starts with the determination of non-relativistic radial functions for the orbitals. In this work, they are computed using the multi-configuration Hartree-Fock (MCHF) approximation [7]. Briefly, the atomic state wave function $\Psi(\gamma\ LS)$ is expanded as a linear combination of configuration state functions (CSFs), denoted by $\Phi(\gamma\ LS)$, so that

$$\Psi(\gamma\ LS) = \sum_i c_i \Phi(\gamma_i\ LS). \tag{6}$$

Each CSF is an antisymmetric sum of products of one-electron spin–orbitals and an eigenfunction of the total orbital momentum and spin angular momentum operators $\mathbf{L}^2$, L_z, $\mathbf{S}^2$ and S_z. The radial functions of the orbitals depend only on the nl quantum numbers, and it is assumed that all spin–orbitals define an orthonormal set.

For each configuration and term the wave function, as given by Eq. 6, included expansions over all CSFs of the form $3d^{10}nln'l'$, where $n \le n' \le 7$ and $l, l' \le 4$ (or g-orbitals) for valence correlation and over CSFs of the form $3d^9 4lnl'$, $n'l''$ for core-valence correlation, with similar limits as for valence correlation. The calculations assumed the same $1s$, $2s$, $2p$, $3s$, $3p$, $3d$ orbitals for all states. These were defined to be the Hartree-Fock (HF) orbitals for the ground state.

A number of strategies may be applied for determining the additional orbitals. Once they are known, they can be used in a configuration interaction calculation with matrix elements computed using the Breit–Pauli Hamiltonian, $H \equiv H_{\mathrm{BP}}$, that includes relativistic operators of order α^2. Some of these operators are diagonal in L and S and are referred to as the relativistic shift [7]. They do not contribute to the mixing of LS terms in the wave function. The remaining operators are diagonal in J. They determine the fine-structure splitting and hence are known as the fine-structure operators. There are three such operators. The spin–orbit operator (s-o) is a one-body operator that produces non-zero matrix elements only between configuration states of the same configuration or between configurations that differ by a single $nl \rightarrow n'l$ excitation. The others are two-body operators, namely spin-other-orbit (s-o-o) and spin–spin (s–s). They can be non-zero between many configuration states that differ by at most two electrons. They become important, for example, when matrix elements of the spin–orbit operator are zero. The eigenstates of a Breit–Pauli interaction matrix represent the expansion coefficients for an atomic state wave function in intermediate or LSJ coupling.

Though expansions in the intermediate coupling approximation could be defined in terms of configurations and all possible couplings for a selected J, in the present work the expansions are defined by LS terms. Thus

$$\Psi(\gamma\ LSJ) = \sum_{LS} \sum_i c_{i,LS} \Phi(\gamma_{i,LS}\ LSJ). \tag{7}$$

In practice, the list of CSFs for a Breit–Pauli calculation is the concatenated list of CSFs for selected terms rather than all possible LS terms for given J and parity.

In addition to the expansions, the results of a calculation depend on the radial functions used for the orbitals. These are assumed to be the same orthonormal set for all LS terms included in the expansion. In order that these be determined optimally, simultaneous MCHF optimization [17] was used for one or more LS terms or eigenstates of a given term. All MCHF calculations were performed using the `atsp2K` atomic structure package [18].

4 Breit–Pauli calculations and results

Table 1 lists the LS expansions included in a Breit–Pauli calculation for groups of atomic states. Only the final calculations included the terms listed in parentheses. Calculations for the $4s^2\ ^1S_0$ ground state and the levels of $4s4p$ were straightforward. Because of the strong configuration interaction between $4s4d$ and $4p^2$ CSFs, optimizing on all terms of $4p^2$ was more complex and several methods were applied.

The $4p^2\ ^3P$ component can have a non-zero interaction with a continuum channel of the same parity and LS. Because $4p^2$ lies below the $3d^{10}4p$ ionization limit, no such background continuum exists and non-relativistic calculations can be performed in the same manner as for a bound state. Thus calculations for $4p^2\ ^3P$ present no problems for the MCHF

Table 1 LS terms included in Breit–Pauli calculations for different eigenstates

Eigenstates		LS terms in the expansion				
$4s^2$	$^1S_0$	^1S	^3P			
$4s4p$	$^3P^o_{0,1,2}$, $^1P^o_1$	$^3P^o$	$^1P^o$			
$4s4d$, $4p^2$	$^3P_{0,1,2}$, $^1D_2$, $^1S_0$	^3P	^1D	^1S		(^1P ^3S ^3D)

method. In our first study of the composition of the $4p^2\ ^3P$ bound component, it was assumed that these ^3P radial functions could be used for all terms when generating the Breit–Pauli interaction matrix for ^3P, ^1D, and ^1S components, and that contributions from ^1P, ^3S, and ^3D as well as any possible interaction with the continuum could be ignored. The energy levels from this calculation are shown in Table 2 and referred to as calculation BP(1). This optimization process for radial functions ignored the strong interaction found earlier [9] between the $4p^2$ and $4s4d\ ^1D$ configuration states. In the calculation denoted by BP(2), radial functions were optimized simultaneously for the lowest ^3P and the three lowest ^1D and ^1S eigenstates. The $4snd$ expansions for ^1D were truncated to include only $4s4d$ and $4s5d$ configuration states so that the dominant component of the third ^1D eigenstate was $4p^2\ ^1D$. Similarly, the expansions for ^1S included only $4s^2$ and $4s5s$ so that the third eigenstate was $4p^2\ ^1S$. The results are shown in Table 2 as BP(2). These results also ignored contributions from ^1P, ^3S, and ^3D. Not listed are the energies of $4s5s\ ^1S$ and $4s5d\ ^1D$. The core-valence expansions that were used ignored the core-valence interaction of the $5l$ electron, for example, and so the energy of $4s5d\ ^1D$ cannot be expected to be as accurate as that for $4s4d\ ^1D$. Also, because of the truncated $4snl$ CSF expansions, these eigenstates represented interactions with the $4snd$ configuration states rather than physical states. In fact, the mean radius of the $5d$ orbital was 166 a_0.

Table 2 compares the Breit–Pauli (BP) energy levels relative to the energy of the ground state from these two calculations with similar observed data [19]. The lower levels appear to be computed more accurately than the higher levels since (BP – obs.) is smaller. By matching the ionization limit instead, we find the largest difference to occur for the lower levels. Furthermore, all energies are too high, thus indicating that the calculations have neglected more correlation in the lower states than in the higher ones, an observation consistent with theory. Relative to the ionization limit, the BP(2) results for $4p^2$ appear to be better. But the fact that the $4p^2\ ^3P_1$ energy level was raised by 450 cm^{-1} when the variational principle was applied simultaneously to seven LS states casts doubt on this conclusion. According to the variational principle, the wave function with the lower energy is the better wave function, and the difference with the observed energy is a reflection of the incompleteness of the correlation included in the computational model.

The larger components of the wave function for $4p^2\ ^3P_2$ and $^1D_2$ are given in Table 3. It should be remembered that this expansion is in terms of a single orthonormal basis for all states and that only $4s$, $4p$, $4d$ are spectroscopic orbitals with the expected nodal structure. The others are variational orbitals from an orthonormal set that minimize the total energy functional. In particular, $4f$ is a contracted orbital with mean radius of 1.39 a_0 whereas $5f$ has about the same mean radius as $5p$. The expansions show the importance of $4p5p$ and $3d^9 4s4p^2$ to both states and of $4p5f$ to the $^1D_2$ state.

These wave functions were then used to compute E1 transitions between all levels. Table 4 reports the transition wavelength (λ, in Å), line strength (S), oscillator strength (f_{ik}), and transition rate (A_{ki}, in s^{-1}), as well as the discrepancy in length and velocity form results of the transition rate (T) in percent. For spin-allowed transitions, T is a reliable accuracy

Table 2 Computed energy levels compared with observed [19] values

Eigenstate		Energy levels (in cm^{-1})			BP(2) - obs.		Energy	
		obs.	BP (1)	BP (2)	(a)[a]	(b)[b]	BP (3)	BSR
$4s^2$	$^1S_0$	0	0	0	0	596		
$4s4p$	$^3P^o_0$	32,311	32,013	32,013	−298	298		
	$^3P^o_1$	32,501	32,193	32,193	−309	287		
	$^3P^o_2$	32,890	32,553	32,553	−337	259		
	$^1P^o_1$	46,745	46,438	46,438	−307	289		
$4s4d$	$^1D_2$	62,459	–	61,969	−490	106	61,985	
$4s$	$^2S_{1/2}$	75,769	–	75,173	−596	0	75,452	
$4p^2$	$^3P_0$	80,175	79,196	79,661	−514	82	79,465	79,459
	$^3P_1$	80,394	79,443	79,893	−501	95	79,677	79,672
	$^3P_2$	80,742	79,821	80,257	−535	61	80,048	80,050
	$^1D_2$	–	94,438	86,198			85,361	84,577
	$^1S_0$	–	92,182	93,933			92,896	92,470

[a] Assuming the same ground state energy
[b] Assuming the same ionization limit

Table 3 Wave function expansions for $4p^2\ {}^3P_2$ and $4p^2\ {}^1D_2$ states of BP(2) calculations

$4p^2$ CSF	$^3P_2$ LS		$4p^2$ CSF	$^1D_2$ LS	
$4p^2$	^3P	0.972	$4p^2$	^1D	0.935
$4p5p$	^3P	−0.153	$4s4d$	^1D	0.202
$3d^9 4s4p^2(^1D)$	^3P	−0.058	$4p5p$	^1D	−0.187
$4p6p$	^3P	−0.049	$4p5f$	^1D	−0.104
$4d6d$	^3P	0.048	$3d^9 4s4p^2(^3P)$	^1D	−0.069
$6d^2$	^3P	0.047	$4s5d$	^1D	0.065
$3d^9 4s4p^2(^3P)$	^3P	−0.042	$4d6s$	^1D	0.059
$4p^2$	^1D	0.040	$6d^2$	^1D	0.048
$3d^9 4s4p(^4P)4f$	^3P	−0.034	$4d6d$	^1D	−0.048
$5p^2$	^3P	−0.034	$5p^2$	^1D	0.043
$4d^2$	^3P	0.031	$4p^2$	^3P	0.041

Table 4 Data for transitions between bound levels in neutral Zn

Multiplet terms		g_i	g_k	λ (Å)	S	f_{ik}	A_{ki} (s^{-1})	T%
$4s^2\ {}^1S$	$4s4p\ {}^3P^o$	1	3	3,106	1.655e−03	1.618e−04	3.729e+04	62
$4s^2\ {}^1S$	$4s4p\ {}^1P^o$	1	3	2,153	1.059e+01	1.493e+00	7.161e+08	3
$4s4p\ {}^3P^o$	$4s4d\ {}^1P^o$	3	5	3,358	3.254e−04	9.810e−06	3.481e+03	59
		5	5	3,400	1.287e−04	2.301e−06	1.328e+03	59
$4s4p\ {}^3P^o$	$4p^2\ {}^3P$	1	3	2,089	3.762e+00	5.471e−01	2.789e+08	2
		3	1	2,109	3.756e+00	1.805e−01	8.140e+08	4
		3	3	2,096	2.818e+00	1.361e−01	2.065e+08	3
		3	5	2,081	4.701e+00	2.288e−01	2.115e+08	2
		5	3	2,112	4.686e+00	1.348e−01	3.357e+08	5
		5	5	2,096	1.403e+01	4.067e−01	6.173e+08	3
$4s4p\ {}^3P^o$	$4p^2\ {}^1D$	3	5	1,852	5.491e−04	3.003e−05	3.505e+04	39
		5	5	1,864	2.585e−02	8.424e−04	1.617e+06	14
$4s4p\ {}^3P^o$	$4p^2\ {}^1S$	3	1	1,620	1.565e−03	9.782e−05	7.462e+05	26
$4s4p\ {}^1P^o$	$4s4d\ {}^1P^o$	3	5	6,439	2.837e+01	4.461e−01	4.306e+07	9
$4s4p\ {}^1P^o$	$4p^2\ {}^3P$	3	1	3,010	2.002e−03	6.735e−05	1.487e+05	22
		3	3	2,989	4.188e−04	1.419e−05	1.059e+04	47
		3	5	2,957	4.679e−02	1.602e−03	7.334e+05	25
$4s4p\ {}^1P^o$	$4p^2\ {}^1D$	3	5	2,515	2.879e+01	1.159e+00	7.332e+08	13
$4s4p\ {}^1P^o$	$4p^2\ {}^1S$	3	1	2,105	3.246e+00	1.561e−01	7.045e+08	16

T is the discrepancy in the length and velocity values of the transition rate, A_{ki}, given in percent. Calculations for the $4p^2$ levels neglected interactions with the continuum

indicator with $4s^2\ {}^1S_0 - 4s4p\ {}^1P^o_1$ and $4s4p\ {}^3P^o_J - 4p^2\ {}^3P_J$ being the most accurate. For intercombination lines, the discrepancy is always larger. Part of this discrepancy is due to the fact that the non-relativistic form of the velocity operator used in Breit–Pauli calculations has not included all of the first-order corrections, but similar discrepancies are also observed in fully relativistic calculations (see Table D of Ref. [20]). In relativistic configuration interaction calculations, it has been shown that the discrepancy is greatly reduced by the inclusion of the contributions from the negative energy sea [21]. Thus it is not clear how this factor can be used as an indicator of accuracy for intercombination lines where fine-structure splitting may be a better indicator.

5 Extensions for photoionization calculations

The bound-state calculations described in the previous section were extended through the use of the B-spline R-matrix method (BSR) [13] for the $4p^2$ resonances in the continuum.

In this method, the energy dependent wave function for a given J is assumed to have the form

$$\Psi(J, E) = \sum_{l,LSJ} \Psi_c(4skl\ LSJ; E) + C(E)\Psi_p(J; E), \quad (8)$$

where $\Psi_c(4skl\ LSJ; E)$ is an energy dependent LSJ channel function and $\Psi_p(LSJ; E)$ represents the expansions for the perturber for a specific J,

$$C(E)\Psi_p(J; E) = \sum_{i,LS} a_{i,LS}(J; E)\Phi(\gamma_i LSJ). \quad (9)$$

The latter expansion includes all configuration states for the bound-state Breit–Pauli calculation for a given J, with those CSFs excluded (such as $4snd$) that could be a basis for the continuum portion. What needs to be computed are the radial functions for the continuum function and the energy dependent $a_{i,LS}(J; E)$ coefficients. The continuum radial functions are approximated by an expansion in terms of a B-spline basis inside a box of radius $R = 60$, and extended to the outer region by R-matrix methods. The BSR method allows orbitals to be non-orthogonal and no orthogonality between the perturber and the channel functions was imposed, except for $\langle 4s \mid ks\rangle = 0$ because the $4s^2$ CSF was included in the perturber expansion. Unlike MCHF, which relies on angular momentum theory to determine energy expressions [18], BSR uses determinantal methods. For CSFs such as $3d^9 4d5d6d$ many terms are generated, largely because of possible overlap integrals. For this reason, only those CSFs were included in a perturber expansion that had a coefficient greater than 0.0001 in magnitude in the normalized Breit–Pauli expansions. Furthermore, the s-o-o and s–s operators of the Breit–Pauli Hamiltonian were only included for the first 2,000 CSFs. In addition, the target expansion retained only those CSFs with coefficients greater than 0.005, raising the ionization limit somewhat.

The MCHF calculations were modified for this extension. As mentioned earlier the $5d$ orbital in the BP(2) calculation represented the interaction of $4p^2\ ^1D$ with high-lying $4snd$ CSFs. In BSR, these interactions would be part of the channel function and a more compact perturber expansion was needed. Consequently, $4s5s$ and $4s5d$ were eliminated from the expansions and the radial orbitals were optimized for $4s4d$ and $4p^2\ ^1D$, $4p^2\ ^3P$, and $4s^2$ and $4p^2\ ^1S$.

Table 5 indicates the operators that may contribute to the interaction between the perturber and the continuum channels. Generally, the Coulomb operators have the largest effect, followed by the spin–orbit operator. Though contributions from the spin-other-orbit are numerous, their overall effect is small. Contributions from Coulomb interactions appear for $J = 0$ and $J = 2$, with the latter including a contribution from the spin–orbit operator. Note that for $J = 1$ the only operator contributing to the interaction between the $4p^2$ CSFs and the continuum channels is the spin-other-orbit operator. Since the effect of correlation between $4p^2\ ^1D$ and $4s4d\ ^1D$ is much stronger than between $4p^2$ and $4s^2$ or $4s5s\ ^1S$, this table suggests an extremely narrow resonance for $4p^2\ ^3P_1$, a narrow resonance for $^3P_0$, a moderate width for $^3P_2$, and wider resonances for $^1S_0$ and $^1D_2$. Experiment, however, has shown the $^3P_1$ level to have a larger width than $^3P_0$. This can be explained in terms of the wave function expansions of Table 3. All levels of $4p^2$ have a $4p5p$ component of about 2%. If this component is treated as part of the zero-order wave function, a first-order relativistic calculation needs to include all the terms of $4p5p$. Thus, in order to get accurate line widths, once the radial functions had been determined, the expansions for ^1D, ^3P and ^1S were concatenated and similar expansions for ^1P, ^3S, and ^3D were added to the Breit–Pauli expansions (see Eq. 7). Together with the MCHF radial orbitals, these CSFs defined the Breit–Pauli interaction matrix. Selected eigenvalues and eigenvectors were determined. Those with coefficients greater than 0.0001 in one or more eigenvectors for $4p^2$ with $J = 0, 1, 2$ defined the J-dependent perturber expansions for the BSR calculations.

Table 5 Types of interactions for different bound configuration state functions and different continuum channels

Bound CSF		Continuum CSF			
		$4skd\ ^1D_2$	$4s4d\ ^3D_J$	$4sks\ ^1S_0$	$4sks\ ^3S_1$
$4s^2$	$^1S_0$	–	–	c	–
$4p^2$	$^1S_0$	–	–	c	–
	$^1D_2$	c	s-o-o	–	–
	^3P_J	s-o-o	s-o-o, s–s	s-o-o	s-o-o
$4s4d$	$^1D_2$	c	s–o, s-o-o	–	–

c Coulomb, *s–o* spin–orbit, *s-o-o* spin-other-orbit, *s–s* spin–spin

Once the energy dependent wavefunctions for $J = 0, 1, 2$ were determined, the positions and widths of the resonances could be determined. The position (E_r) and the width (Γ) of a resonance can be extracted by fitting $C(E)^2$ to a Lorentzian profile, i.e.,

$$C(E)^2 = \frac{1}{\pi}\frac{\frac{1}{2}\Gamma}{(E - E_r)^2 + \frac{1}{4}\Gamma^2}. \quad (10)$$

Figure 1 shows a plot of $C(E)^2$, on a logarithmic scale, for the three even parity $J = 0, 1, 2$ continuum wave functions as a function of the energy of the contiuum electron or, equivalently, the energy relative to the ionization limit. Note the overlapping $4p^2\ ^1D_2$ and $4p^2\ ^3P_2$ resonances. The former has a relatively low height over a broad range, whereas the latter is a well-defined resonance of moderate height. The width of $^1D_2$ was not accurately determined. The energy of

Table 6 The positions (E_r) and width (Γ) at half height for the $4p^2$ resonances in cm^{-1}

Term	Present			Ref. [2]		Ref. [12]
	E_r(BP(3))	E_r(BSR)	Γ	E_r	Γ	Γ
$^3P_0$	4,013	4,007	0.072	4,406[a]		<0.020
$^3P_1$	4,225	4,220	0.243	4,625[a]		0.36 ± 0.05
$^3P_2$	4,596	4,598	21.46	5,023[a]	21.7[a]	22.2 ± 0.5
$^1D_2$	9,909	9,125	8517.0		6,800	
$^1S_0$	17,444	17,018	629.2		<170	

The position is relative to an ionization limit: 75,452 cm^{-1} for BP(3) and BSR, 75,769 cm^{-1} for Ref. [2]
[a] Experimental values from Ref. [2]

the continuum electron is given in eV below the graph and in cm^{-1} above the graph in order to relate the graph to the data of Table 6.

Table 6 reports the positions and widths of the $4p^2$ resonances and compares these with other data. Included with the present results are positions of the resonances in calculations that ignore the continuum [BP(3)] and in calculations (BSR) that include the $4sns/ks$ or $4snd/kd$ channels. For the levels of ^3P, the differences in positions are small, but the position of $^1D_2$ has been significantly affected by the interaction with $4snd/kd$. For $^1S_0$ the interaction with $4sns/ks$ has been considerably less. In both cases, the position has been lowered. These positions are reported relative to the computed $4s\ ^2S_{1/2}$ ionization limit whereas the positions of the observed levels are reported with respect to the observed ionization limit. These shifts (399, 405, 425 cm^{-1}), respectively, are a reflection largely of the different values for the ionization limits. The computed line width for the $^3P_2$ is in good agreement with the value reported by Martin and Kaufman. They obtained their value by measuring the width of a microphotometer trace at half the peak intensity for the $4s4p\ ^3P^o_1 - 4p^2\ ^3P_2$ transition. Chantpie et al. [12] investigated the $4s4p\ ^3P^o_J - 4p^2\ ^3P$ resonances using an optogalvanic detection method as well as through single configuration, fully relativistic calculations. Their theoretical results were in agreement with their experimental values reported in Table 6. They found the line width for $4p^2\ ^3P_1$ to be greater than that for $^3P_0$. Aymar et al. [22] argued that, in Cd, the line width was affected by the difference in the $5p_{1/2}$ and $5p_{3/2}$ orbitals, which is accounted for naturally in a fully relativistic calculation. In $4p^2\ ^3P_1$ the most important interaction was found to be the Coulomb interaction with the $4sks\ ^3S_1$ continuum. In our Breit–Pauli approach, this effect can be interpreted as a second-order cross-interaction between the spin–orbit operator and the Coulomb operator, namely $\langle 4p^2\,^3P_1 \mid H_{s-o} \mid 4p5p\,^3S_1\rangle\langle 4p5p\,^3S_1 \mid H_{\rm coulomb} \mid 4sks\,^3S_1\rangle$. The present calculations confirm that this interaction is larger than the interaction of the bound component for the $J = 0$ channel with its continuum, namely $\langle c_1 4s^2 + c_2 4p^2\,^1S_0 \mid H \mid 4sks\,^1S_0\rangle$. This interaction includes the coulomb interaction that usually is larger than the spin–orbit interaction (see Table 5). For the $^1D_2$ and $^1S_0$ resonances, the line width values from Ref. [2] were estimated from trends along the sequence of $F^2(4p, 4p)$ Slater integrals and are approximate at best.

6 Photoionization cross sections

Once the energy dependent wave functions for the different J-values were determined for the continuum region, the Breit–Pauli wave functions for the initial states were recomputed in the Condon and Shortley phase conventions needed by the BSR code and then used to compute the photoionization cross sections.

Figure 2 shows the total cross section to $4p^2\ ^3P$ for photoionization from different $4s4p$ initial states as a function of the continuum electron energy. The latter is also the total energy relative to the ionization limit as well as the energy of the ejected electron. Note the very narrow resonance to $^3P_0$, the noticeable width of $^3P_1$ and the significant width of $^3P_2$. For $^3P^o_J$ initial states the cross section for transitions to $^3P_2$ do not exhibit cancellation, whereas the cross section for excitation from the $^1P_1$ initial state vanishes (has a zero) near the position of the $^3P_2$ resonance.

Figure 3 shows the length and velocity forms of the total cross section for photoionization from the $4s4p\ ^1P^o_1$ level on a logarithmic scale. Note the very broad cross section for contributions from the $4p^2\ ^1D_2$ region and the excellent agreement in length and velocity forms for the $J = 0 - 2$ continua.

Finally, in Fig. 4 total cross sections for photoionization from $4s4p$ levels are shown as a function of the wavelength.

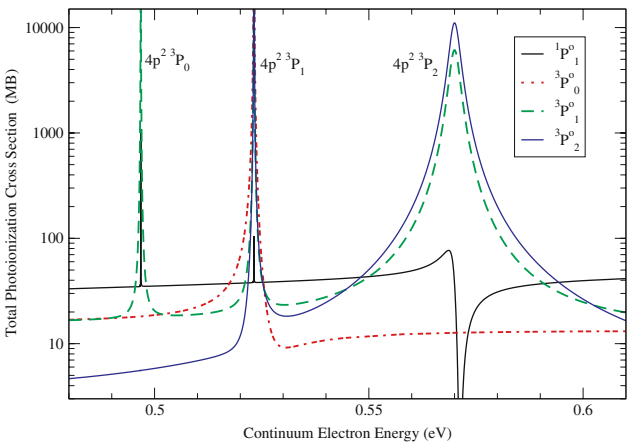

Fig. 2 Total photoionization cross sections in the region of $4p^2\ ^3P_J$ resonances as a function of the energy (in eV) of the continuum electron for different initial states

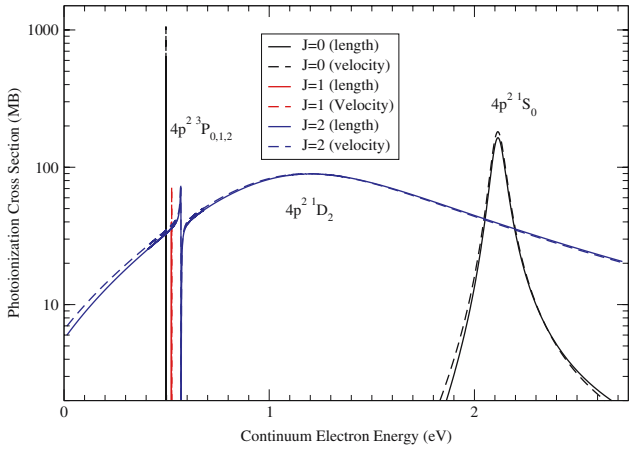

Fig. 3 Photoionization cross sections for excitation from the $4s4p\ ^1P^o_1$ level as a function of the continuum electron energy (eV)

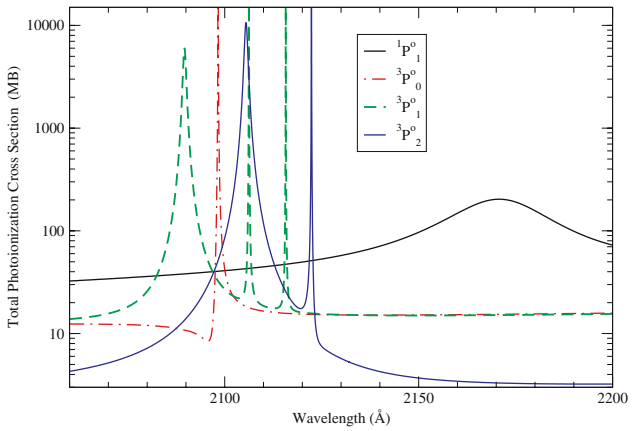

Fig. 4 Total photoionization cross sections for excitation from different initial states to $4p^2$ resonances as a function of wavelength

There are two moderately broad resonances, namely $^3P^o_{1,2} - {}^3P_2$. The broad resonance at about 2,175 Å is $^1P^o_1 - {}^1S_0$. The others are narrow lines with the $^3P^o_1 - {}^3P_1$ line overlapping the broad $^3P^o_2 - {}^3P_2$ line.

7 Conclusion

Even in neutral Zn, relativistic effects are important in the calculation of cross sections for photoionization from $4s4p$ levels to the $4p^2$ resonances. A Breit–Pauli calculation required the inclusion of all terms of $4p5p$ in the perturber expansions and not only those of $4p^2$. The additional terms improved the $4p^2\ ^3P_0 - {}^3P_1$ energy separation from 232 cm^{-1} (BP(2)) to 212 cm^{-1} (BP(3)), compared with 219 cm^{-1} for observed [2]. The relative position of these levels is not significantly affected by high-lying Rydberg CSFs nor by the continuum. In this study we did not investigate the use of non-orthogonal orbitals for perturbers or the introduction of additional target states such as $3d^{10}4p\ ^2P^o$.

Acknowledgments This paper is dedicated to the memory of Professor Serafin Fraga for his contributions to theoretical and computational formulations for the prediction of properties of many-electron atomic systems within the framework of configuration interaction treatments in quantum chemistry, ranging from simple relativistic atoms to complex protein structures. Oleg Zatsarinny acknowledges support from the US National Science Foundation under grant PHY-0555226.

References

1. Sawyer RA, Reese NC (1925) Nature 116:936
2. Martin WC, Kaufman V (1970) J Opt Soc Am 60:1096
3. Selwyn EW (1929) Proc Phys Soc (Lond) 41:392
4. Majorana E (1931) Nuovo Cimento 8:107
5. Shenstone AG (1931) Phys Rev 38:873
6. Fano U (1961) Phys Rev A 124:1866
7. Froese Fischer C, Brage T, Jönsson P (1997) Computational atomic structure: an MCHF approach. Inst. of Physics Publishing, Bristol
8. Froese Fischer C, Hansen JE (1978) Phys Rev A 17:1956
9. Froese Fischer C, Hansen JE (1979) Phys Rev A 19:1819
10. Curtis LJ (1992) J Opt Soc Am B 9:5
11. Cheng T-C, Huang K-N (1992) Phys Rev A 45:4367
12. Chantepie M, Cheron B, Cojan JL, Landais J, Laniepce B, Aymar M (1988) J Phys B 21:1379
13. Zatsarinny O (2006) Comput Phys Commun 174:273
14. Cowan RD (1981) The theory of atomic structure and spectra. University of California, Berkeley
15. Karazija R (1996) Introduction to the theory of X-ray and electronic spectra of free atoms. Plenum Press, New York and London
16. Brage T, Froese Fischer C, Miecznik G (1992) J Phys B 25:5289
17. Tachiev G, Froese Fischer C (1999) J Phys B 32:5805
18. Froese Fischer C, Tachiev G, Gaigalas G, Godefroid MR (2007) Comput Phys Commun (in press)
19. Ralchenko Yu et al. (2007) NIST atomic spectra dababase, (http://www.physics.nist.gov/PhysRefData/ASD/)
20. Froese Fischer C, Tachiev G, Irimia A (2006) At Data Nucl Data Tables 92:607
21. Chen MH, Cheng KT, Johnson WR (2001) Phys Rev A 64:042507
22. Aymar M, Luc-Koenig E, Chantepie M, Cojan ML, Landais J, Laniepce B (1986) J Phys B 19:3881